by a strong anomaly of the Indian Ocean dipole (IOD), the main cause of extreme droughts over Australia (Ummenhofer et al. 2009). The exceptional severity of the Australian fires is highlighted in Plate 2.1y, which shows the number of days with daily AOD at 550 nm above 99.9% of the daily record between 2003 and 2018. Sidebar 7.6 discusses these fires in more detail.

Radiative forcing resulting from aerosol–radiation (RFari) and aerosol–cloud interactions (RFaci) for the period 2003–19 is shown in Fig. 2.52, as estimated using the methods described in Bellouin et al. (2020). The year 2019 was close to the long-term average in terms of both RFari and RFaci. Time series indicate no statistically significant trends in aerosol radiative forcing because the radiative impact of decreasing trends over Europe, North America, and China is offset by increasing trends over India. Evaluating trends remains statistically challenging because of large uncertainties in the estimates, which are mostly due to lack of knowledge of the anthropogenic fraction of the aerosol and its radiative forcing efficiency.

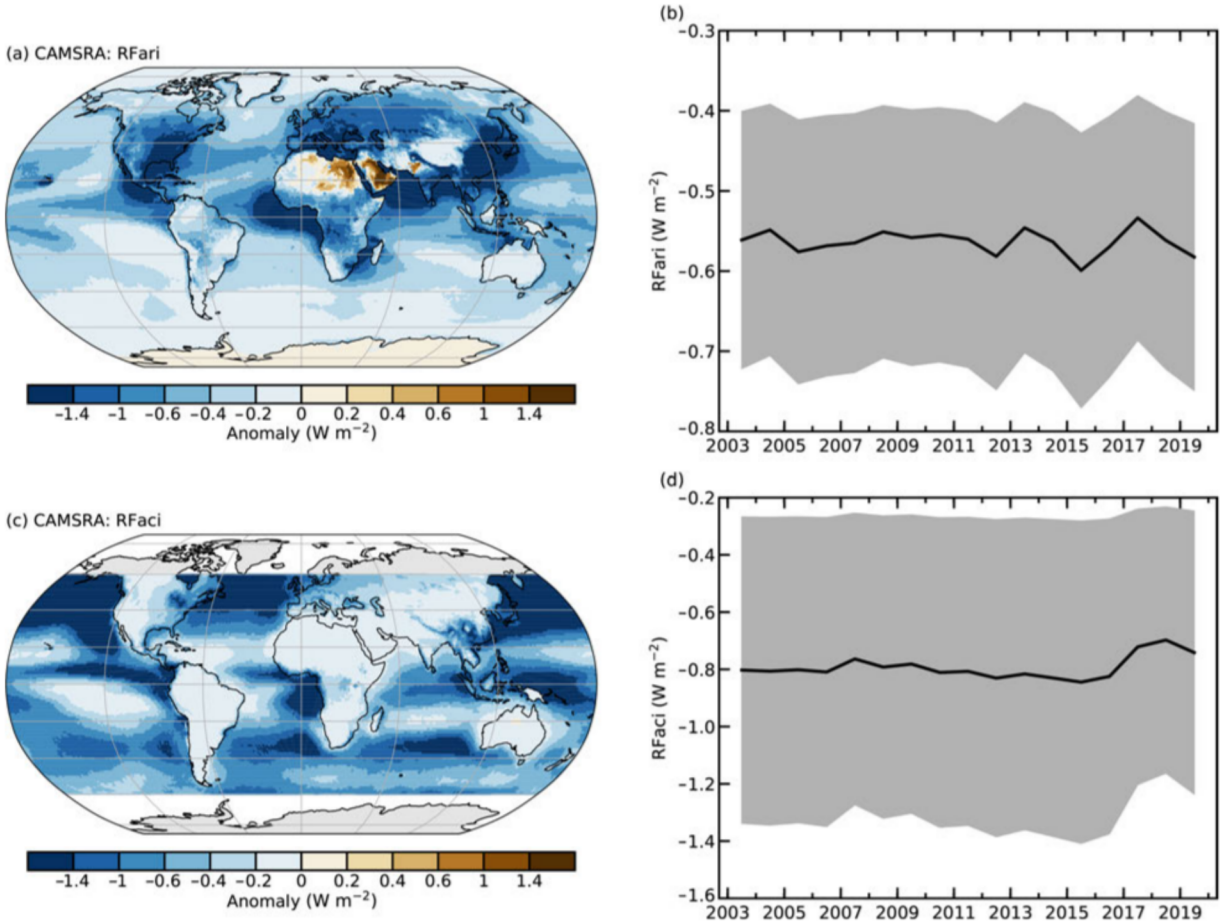

Fig. 2.52. Radiative forcing in the shortwave spectrum of (a), (b) aerosol-radiation (RFari) and (c), (d) aerosol-cloud interactions (RFaci) for 2003–19. The left column shows the average distribution. The right column shows time series of global averages, with the uncertainties of these estimates shown in gray.

4) Stratospheric ozone—M. Weber, W. Steinbrecht, C. Arosio, R. van der A, S. M. Frith, J. Anderson, M. Coldewey-Egbers, S. Davis, D. Degenstein, V. E. Fioletov, L. Froidevaux, D. Hubert, C. S. Long, D. Loyola, A. Rozanov, C. Roth, V. Sofieva, K. Tourpali, R. Wang, and J. D. Wild

The ozone layer that protects the biosphere from the harmful effects of ultraviolet radiation (UV) resides in the stratosphere. The total ozone column, with its main contributions from lower stratospheric ozone, determines how much UV reaches the surface. Over recent decades, changes in the upper stratospheric ozone have shown the clearest signs of ozone recovery due to the phasing out of ODSs since the late 1980s, following the Montreal Protocol (section 2g2). The total ozone

column annual mean anomaly distribution for 2019 in Plate 2.1z shows opposite behavior in the two hemispheres. While the Southern Hemisphere (SH) shows positive anomalies with respect to the long-term mean, steadily increasing towards the South Pole and over Australia, negative anomalies cover most of the Northern Hemisphere (NH) with some positive values, mostly at high

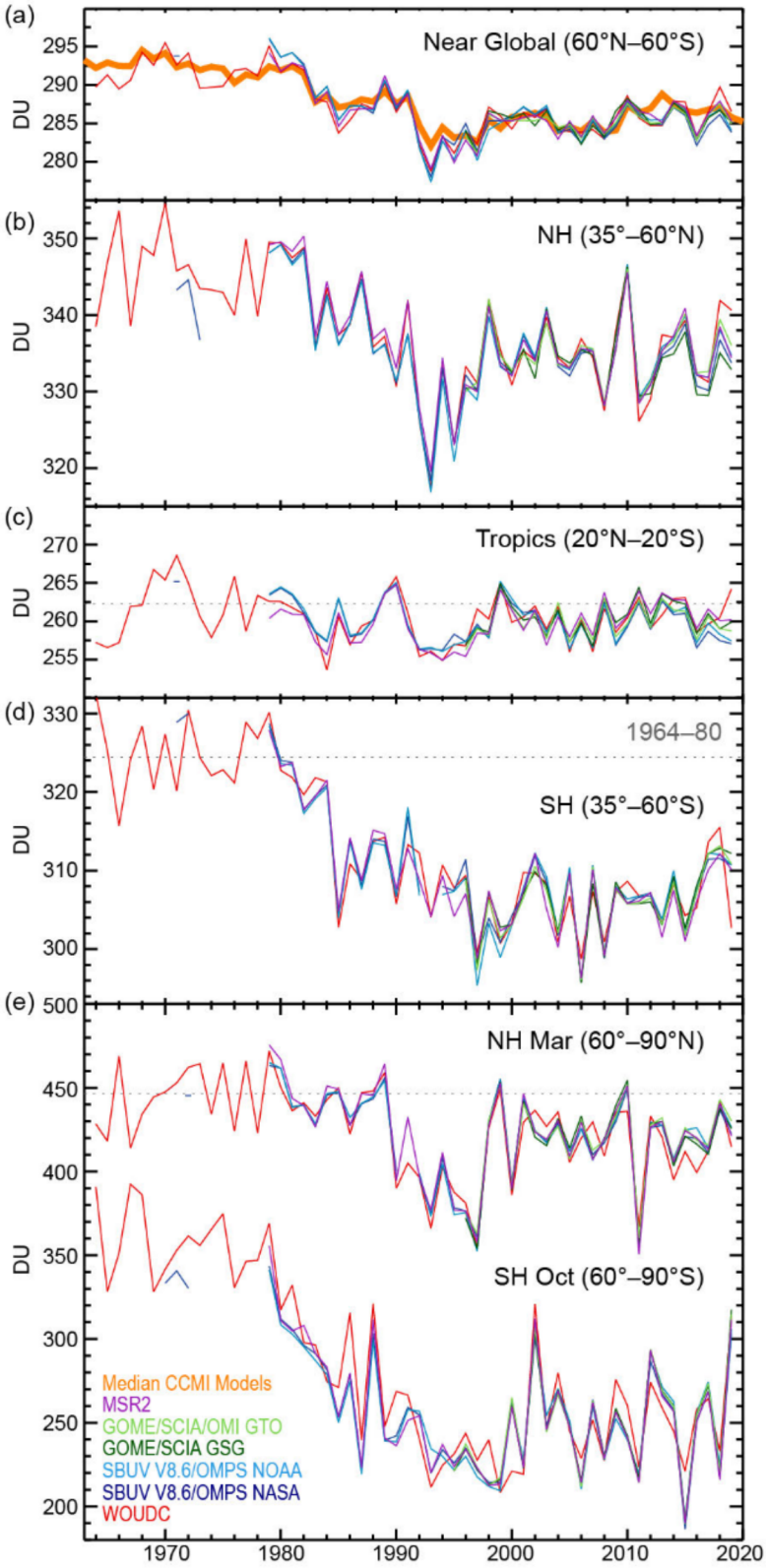

Fig. 2.53. Time series of annual mean total ozone (DU) in (a)–(d) four zonal bands, and (e) polar (60°–90°) total ozone in Mar (NH) and Oct (SH), the months when polar ozone losses usually are largest. Data are taken from WOUDC (World Ozone and Ultraviolet Radiation Data Centre) ground-based measurements combining Brewer, Dobson, SAOZ (Système D'Analyse par Observations Zénithales), and filter spectrometer data (red; Fioletov et al. 2002; 2008); the BUV/SBUV/SBUV2 V8.6/OMPS merged products from NASA (MOD V8.6, dark blue; Frith et al. 2014, 2017) and NOAA (light blue; Wild and Long, pers. comm., 2019); the GOME/SCIAMACHY/GOME-2 products GSG from University of Bremen (dark green; Weber et al. 2018) and GTO from ESA/DLR (light green, Coldewey-Egbers et al. 2015; Garane et al. 2018). MSR-2 (purple) assimilates nearly all ozone datasets after corrections with respect to the ground data (van der A et al. 2015). All six datasets have been bias corrected by subtracting averages for the reference period 1998–2008 and adding back the mean of these averages. The dotted gray lines in each panel show the average ozone level for 1964–80 calculated from the WOUDC data. The thick orange lines shows the average from chemistry-climate (CCMI) model runs (Eyring et al. 2013; Morgenstern et al. 2017; WMO 2018; SPARC/IO3C/GAW 2019). All observational data for 2019 are preliminary.

northern latitudes. Total ozone levels vary from year to year, depending on the dynamical state of the global atmosphere mainly determined by El Niño–Southern Oscillation (ENSO) and the Quasi-Biennial Oscillation (QBO). Both ENSO and the QBO are tropical phenomena that have a strong influence on the Brewer-Dobson circulation (BDC) determining the global stratospheric ozone distribution (e.g., Diallo et al. 2018; Olsen et al. 2019). Throughout 2019, the QBO was in its west phase, which generally leads to higher total ozone in the inner tropics and lower ozone in the subtropics and beyond (Plate 2.1z). The extended regions of below-average total ozone at low to middle NH latitudes are possibly linked to the weak ENSO condition in 2019 (Olsen et al. 2019). A major feature of 2019 is the very weak stratospheric SH winter polar vortex, a very small ozone hole (see Sidebar 6.1), and above-average total ozone at high southern latitudes during austral winter/spring as well as in the annual mean (Plate 2.1z). During the 2019 Antarctic winter/spring season, a stratospheric warming event, which is rare in the SH but frequent in the NH, strongly perturbed the polar vortex. A persistent weak polar vortex in winter/spring, as in 2019, is associated with a stronger hemispheric BDC, occurring usually during west QBO phases, that leads to more ozone being transported into middle to high latitudes throughout much of the SH. In addition, higher polar winter stratospheric temperatures also reduce polar chemical ozone loss (e.g., Weber et al. 2011). As a consequence, annual mean total ozone in 2019 was fairly high, by up to 65 DU above the long-term average, at high southern latitudes (Plate 2.1z).

Figure 2.53 displays the annual mean total column ozone time series from various merged datasets for the near-global (60°N–60°S) average, tropics, extratropics, and selected months in the polar regions. In October 2019, the SH polar cap total ozone (Fig. 2.53e) was as high as in 2002 and 1988, both years characterized by high dynamical activity and perturbed winter vortices (Schoeberl et al. 1989; Sinnhuber et al. 2003) and about 100 DU above the value in October 2015, a year with substantial polar ozone loss (Solomon et al. 2016). On the global scale (Fig. 2.53a), total ozone mean values in 2019 were lower than the previous year but within the variability observed during the last two decades. The same is true for the NH midlatitudes and the tropics (Figs. 2.53b,c) while midlatitude SH values were above the post-1990 average (Fig. 2.53d). In Fig. 2.53a, the median of 17 climate-chemistry model CCMI runs are also shown (Eyring et al. 2013; Morgenstern et al. 2017; WMO 2018; SPARC/IO3C/GAW 2019). The agreement of the observations with models that account for changes in ODS and greenhouse gases gives strong evidence that total ozone is on its slow path of recovery. However, in 2019 and previous years, the global ozone means from observations, as well from the CMI models, are still about 3% below the average from the period 1964–1980, when ODS levels were low.

Figure 2.54 shows ozone changes at two different altitudes, in the upper stratosphere (panels a–c, 42 km altitude) and in the lower stratosphere (panels d–f, 22 km). Ozone in the upper stratosphere shows the larger decline due to ODS increases until the late 1990s (WMO 2018). This large decline was stopped as a result of measures mandated in the international Montreal Protocol to phase-out ODS. Since about 2000, we have been in a phase of slow ozone recovery. In 2019, ozone values in the upper stratosphere were above the 1998–2008 average. In the lower stratosphere, long-term ozone variations are dominated by meteorological variations and transport (e.g., Chipperfield et al. 2018). Figures 2.54d–f show no clear sign of ozone increases in the lower stratosphere over the last 20 or so years. In 2019, the lower stratospheric values were at the lower end of expectations (gray shaded area of model predictions) in the NH and tropical bands (Figs. 2.54d,e). The continuing tropical decline (20°N–20°S) has been linked to climate change-related acceleration of the meridional BDC (Ball et al. 2018; Chipperfield et al. 2018; WMO 2018). Large interannual variations, as well as uncertainties in the observational data records (spread between different datasets), make reliable detection of the expected small underlying trends rather difficult, especially in the lower stratosphere.

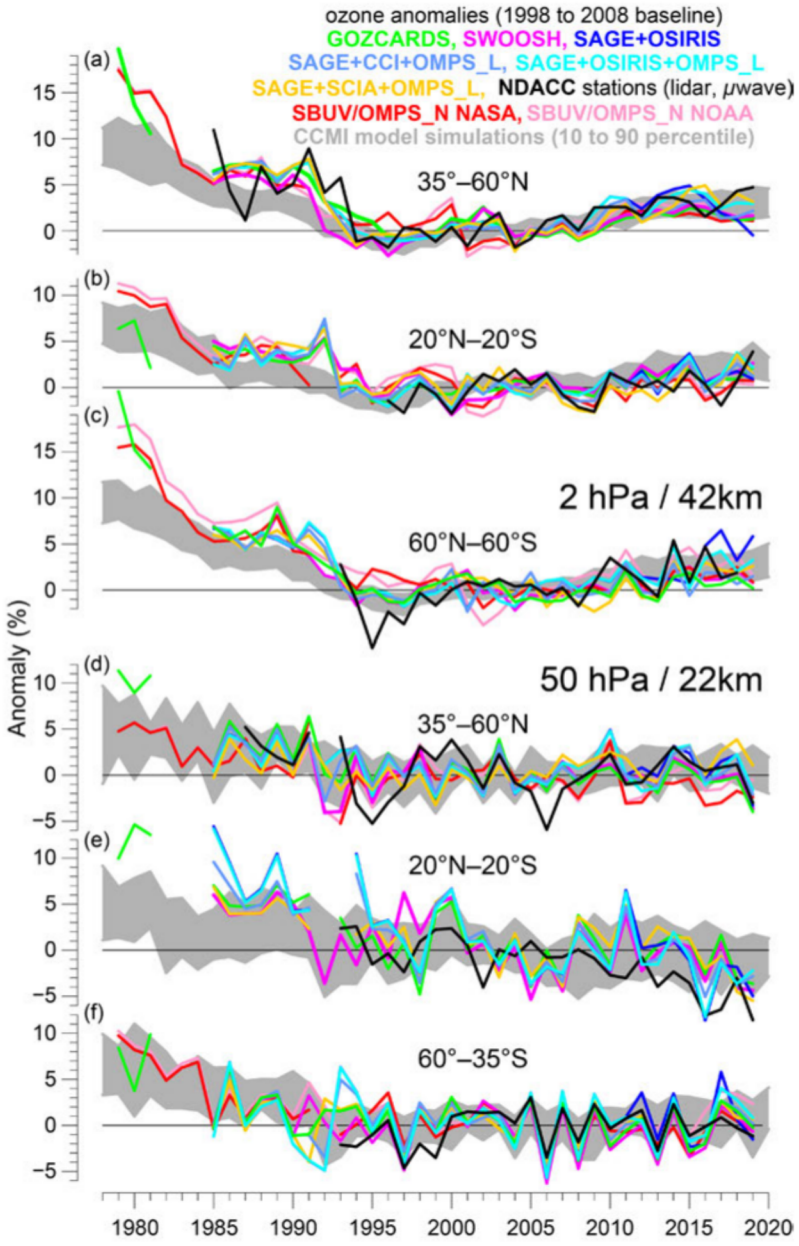

Fig. 2.54. Annual mean anomalies of ozone in the upper stratosphere (a)–(c) near 42 km altitude or 2 hPa pressure and in the lower stratosphere (d)–(f) near 22 km or 50 hPa, for three zonal bands: 35°–60°N, 20°N–20°S (tropics), 35°–60°S, respectively. Anomalies are referenced to the 1998–2008 baseline. Colored lines are for long-term records obtained by merging different limb (GOZCARDS, SWOOSH, SAGE+OSIRIS, SAGE+CCI+OMPS-L, SAGE+SCIAMACHY+OMPS-L) or nadir viewing (SBUV, OMPS-N) satellite instruments. Black line is from merging ground-based ozone records at seven NDACC stations employing differential absorption lidars and microwave radiometers. See Steinbrecht et al. (2017), WMO (2018), and Arosio et al. (2018) for details on the various datasets. Gray-shaded area shows the range of chemistry-climate model from CCMI (WMO 2018; SPARC/IO3C/GAW 2019; Dhomse et al. 2018). Ozone data for 2019 are not yet complete for all instruments and are still preliminary.

5) Stratospheric water vapor—S. M. Davis, K. H. Rosenlof, D. F. Hurst, H. Vömel, and H. B. Selkirk

Stratospheric water vapor (SWV) is a radiatively and chemically important trace gas with its variability strongly affected by the absolute humidity of air entering the stratosphere in the tropics, which is in turn largely determined by the temperature of the tropical cold point tropopause. Following 2018, a year in which lower stratospheric water vapor in the tropics dropped to a near-record low for the *Aura* Microwave Limb Sounder (MLS) satellite record (2004–19), water vapor abundance in the tropical lower stratosphere increased slightly during 2019 (Fig. 2.55). In January 2019, the *Aura* MLS monthly mean tropical (15°N–15°S) lowermost SWV anomaly (at 82 hPa, or ~17 km) was −0.6 ppm (parts per million, equivalent to a mole fraction of μmol mol^{-1}), about 20% below the 2004–19 January average. The tropical lower SWV anomaly transitioned to positive in April and remained between +0.3 and +0.4 ppm (within 10% of the average value for each month) for the remainder of the year (Fig. 2.55).

In general, the qualitative behavior of lowermost SWV observed by *Aura* MLS is consistent with balloon-borne frost-point hygrometer soundings at five locations (Fig. 2.56), although a small drift in MLS relative to the balloon measurements noted in earlier work persists (Hurst et al. 2016). The